ELSEVIER

Materials Science and Engineering A356 (2003) 81–92

MATERIALS SCIENCE & ENGINEERING A

www.elsevier.com/locate/msea

Effects of loading frequency on fatigue crack growth mechanisms in α/β Ti microstructure with large colony size

F. Sansoz, H. Ghonem *

Department of Mechanical Engineering, Mechanics of Materials Laboratory, University of Rhode Island, Kingston, RI 02881, USA

Received 8 January 2002; received in revised form 2 January 2003

Abstract

This paper deals with crack tip/microstructure interactions at 520 °C in lamellar Ti–6Al–2Sn–4Zr–2Mo–0.1Si (Ti6242) alloy under different fatigue loading frequencies. A series of heat treatments were performed in order to produce large colony microstructures that vary in their lamellar and colony size. Fatigue crack growth (FCG) experiments were conducted on these microstructures at loading frequencies of 10 and 0.05 Hz. The lower frequency was explored with and without imposing a 5 min hold-time at the peak stress level during each loading cycle. Results show that the crack growth behavior is sensitive to the loading frequency. For the same microstructure, the crack growth rate is found to be lower at 10 than at 0.05 Hz. The addition of a hold-time, however, did not alter the FCG rate indicating that creep strain during one loading cycle does not contribute significantly in the crack growth process. It is also shown that variations in lamella and colony size have no effects on the FCG rate except for the early stage of crack propagation. Scanning Electron Microscope examinations are performed on the fracture surface in order to identify the relevant crack growth mechanisms with respect to the loading frequency and the microstructure details. Quasi-cleavage of the α/β colonies along strong planar shear bands is shown to be a major mode of failure under all test condition. At a loading frequency of 10 Hz, the crack path proceeds arbitrary along planes either perpendicular or parallel to the long axis of α lamellae, while at 0.05 Hz, parallel-to-lamellae crack paths become favored. Corresponding differences of crack growth behavior are examined in terms of slip emission at the crack tip and interactions with the microstructure details.

Keywords: Fatigue crack growth; Fracture mechanisms; Quasi-cleavage; Loading frequency effects; Large colony microstructure; α/β lamellar titanium alloys

1. Introduction

The α/β and near-α titanium alloys are extensively used in the manufacturing of compressor disks for commercial and military aero-engines [1]. For that reason, a considerable amount of research has been devoted to the microstructure details and processing routes of these alloys [2], as well as to the relationship between microstructure and associated mechanical properties at elevated temperature [3–5]. Different investigations [4,6–10] have established that fully lamellar Ti microstructures, produced by β-forging and heat-treatment, have higher creep resistance, fracture toughness and long fatigue crack growth (FCG) behavior than α/β-processed materials. Fully lamellar microstructures consist of α platelets separated by retained β lamellae and arranged in Widmanstätten formation, or in colonies of similarly aligned platelets. These colonies, in turn, are formed upon quenching from β solutioning of the prior β grains. Decreasing the content of β stabilizing elements, as achieved in high temperature Ti alloys, increases the tendency to transform the microstructure into large colonies of α platelets (0.1–1 mm) [11]. Yoder et al. [12,13] placed particular emphasis on the role played by the colony size in affecting the FCG behavior. For ΔK value lower than a transition point, the fatigue cracking is found increasingly sensitive to microstructure details and dominated by strong planar shear bands, which results in fracture surfaces with a faceted morphology and significant crack path bifurcation [12]. This appears, particularly, when the reversed

* Corresponding author.
E-mail address: ghonem@egr.uri.edu (H. Ghonem).

0921-5093/03/$ - see front matter
doi:10.1016/S0921-5093(03)00112-6

plastic zone is as small as the colony size. It was suggested that in fully lamellar microstructure, the colony size controls the effective slip length in an activated system assuming that the Burgers' orientation relationships allow easy slip transmission at α/β interfaces [9]. According to this, the propagation rate of a micro-crack will increase as the slip length increases, and the colony boundaries become strong obstacles to propagation. Eylon and co-workers [4,11,14–17] have carried out studies in order to investigate the FCG rate in large colony Ti microstructures, i.e. when reversed plastic zone size is significantly smaller as compared to colony size. These authors pointed out that not only the size but also the orientation of the colonies of similarly aligned α platelets, are dominant factors in the FCG behavior, since intense shear bands developing ahead of the crack are highly influenced by microstructure orientation. Yuen et al. [18] proposed that, when the cyclic plastic zone size is less than a colony diameter, initial yielding and reversed shear must be confined to a limited number of slip system, and cracking, afterward, proceeds in a similar manner to stage I fatigue crack initiation and propagation. It was indicated also by Eylon et al. [16] that in large α/β colonies, the FCG process might be interpreted by start/stop behavior at colony boundaries; the stopping event being the re-initiation of cracking to the next colony. Ravichandran [19], however, concluded that α platelets are predominant microstructure features in fully lamellar microstructures, while colonies are more important in Widmanstätten formation only. Choi et al. [20] showed also that FCG rates could be reduced by α/β interface cracking. Therefore, it appears that no consensus is achieved with regard to the relative importance of colony microstructure features in the operating damage mechanism.

In alloys for compressor disks, the FCG mechanism is further complicated since high temperature, low loading frequency and hold-time effects may operate simultaneously, and are likely to affect the crack tip deformation region. Subsequently, this makes the identification of a controlling microstructure feature more difficult. It has been observed in large colony microstructures under low cycle fatigue testing, that the significance of cracking initiating parallel to α/β interfaces increases as temperature increases or loading frequency decreases [21]. The latter effect, i.e. the role of small loading frequency (<10 Hz) has been examined in relation to the FCG rate in different Ti alloys. It is found that the FCG rate increases as the frequency decreases [22]. This has been related to different mechanisms including creep-fatigue interactions [23,24], strain rate dependency [25] and/or crack tip environmental degradation [26–29]. The interactions between microstructure, crack-tip growth process and loading frequency, however, are not fully understood in titanium microstructure with large colonies.

The primary objective of this paper is to explore the effects of small loading frequency (0.01–10 Hz) on FCG in well-controlled lamellar α/β microstructures with large colonies. Crack-tip interactions with the underlying microstructures are studied in an effort to better understand the micro-mechanisms of fatigue at a temperature close to maximum operation conditions for the α/β titanium alloys that are used in aero-engines. The model material is the α/β alloy Ti–6Al–2Sn–4Zr–2Mo–0.1Si (Ti6242). In the present work, all tests were conducted at 520 °C. The first part of this paper briefly reviews the relationships between heat treatment procedure and microstructure, and presents three typical fully lamellar microstructures, which are used in this work. The results of the FCG experiments performed on each of these microstructures are also presented. The second part focuses on the examinations of the controlling crack growth mechanisms with particular emphasis on the orientation of crack path with respect to the microstructure details and different loading frequencies.

2. Experimental procedure and results

The first part of this section describes the steps of heat treatment that affect the microstructure of lamellar Ti alloys and details the procedure to produce the different microstructures used in this study. This is followed by a description of the FCG experiments.

The material used in this investigation was obtained from a manufactured compressor disk forged at 30 °C above the β transus (995 °C). Its chemical composition is: Ti-balance, Al-6.000, Sn-1.940, Zr-4.095, Mo-2.045, Si-0.115, Fe-0.031, C-0.009, O-0.011 (in wt.%). The as-received microstructure presents an arrangement of relatively large α/β lamellar colonies (~ 100 μm), as shown in Fig. 1. Note in this figure that the prior-β grains are hardly discernable and small α phase 'globules', which may have resulted from recrystallisation during forging [30], are located at the triple point of adjacent colonies. A series of heat treatments were performed on this microstructure in order to control the size of the microstructure features. The typical route was a solutioning of 1 h at 1025 °C followed by quenching at room temperature. The material was then aged for 8 h at 595 °C and air-cooled. The role of aging in Ti6242 alloy is to help thermal stability and precipitation of small Ti_3Al particles for strengthening. It is difficult to reduce the grain size with conventional heat treatment procedures, except when the material is hot-rolled in the α/β field and after a short β annealing [31]. Semiatin et al. [32] also obtained a grain size less than 40 μm with rapid heating rates (>100 °C s^{-1}) up to supertransus temperatures on VT9 alloy, of similar

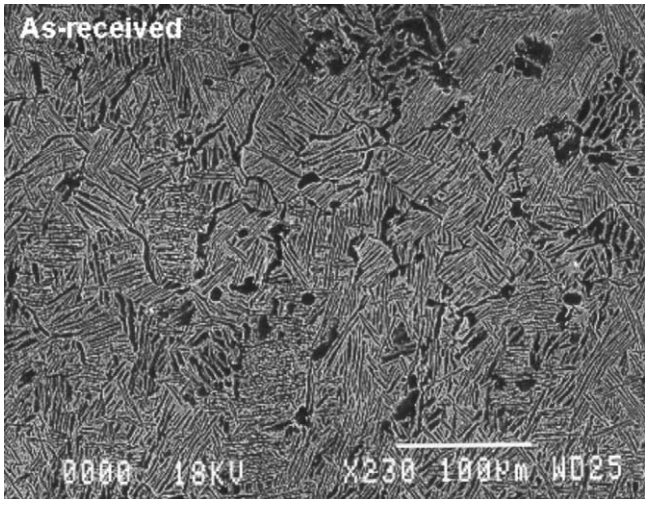

Fig. 1. Microstructure of as-received β-forged Ti6242 alloy.

chemical composition than Ti6242 alloy. In the present study, no attempts were made to vary the β grain size. It is known, however, that both the size of α-platelets and α/β colonies are dependent on the cooling rate after the solutioning treatment; the platelets and colony size increase as the cooling rate decreases [9]. Three different cooling rates were, therefore, imposed: air-cooling (134 °C min^{-1}), furnace cooling (10 °C min^{-1}), and very slow furnace cooling (1 °C min^{-1}). The resulting microstructures are shown in Fig. 2. Microscopic examinations were made using scanning electron microscopy (SEM) and optical microscopy. Quantitative measurements were conducted in order to determine the size of the prior β grain, the α/β colony, and the α and β platelets on each microstructure. The grain size and the α/β colony size were measured using the mean intercept method over 20 features, respectively. The size of the α and β platelets was estimated by taking the average distance over ten platelets measured in different colonies. These results are reported in Fig. 3 as a function of the cooling rate. The size of the prior-β grains is kept very large (0.8 mm) and approximately constant in all microstructure as shown in Fig. 3(a). Fig. 3 shows also that the most significant effect of the cooling rates occurs in the dimension of the colony and the α platelets. In this paper, the three microstructures discussed above will be referred to as fine lamellar, coarse lamellar, and extra-coarse lamellar microstructures. In these microstructures, the average thickness of α platelets is 0.7, 2.0 and 5.9 μm, and the average diameter of colonies is 0.11, 0.2 and 0.46 mm, respectively. The average thickness of the β lamellae is found to be similar in all produced microstructures and equal to 0.2 μm; see Fig. 3(b).

FCG experiments were conducted using Compact Tension specimens, CT12.5 ($B = 6.35$ mm and $W =$ 25.4 mm) machined from the three different micro-

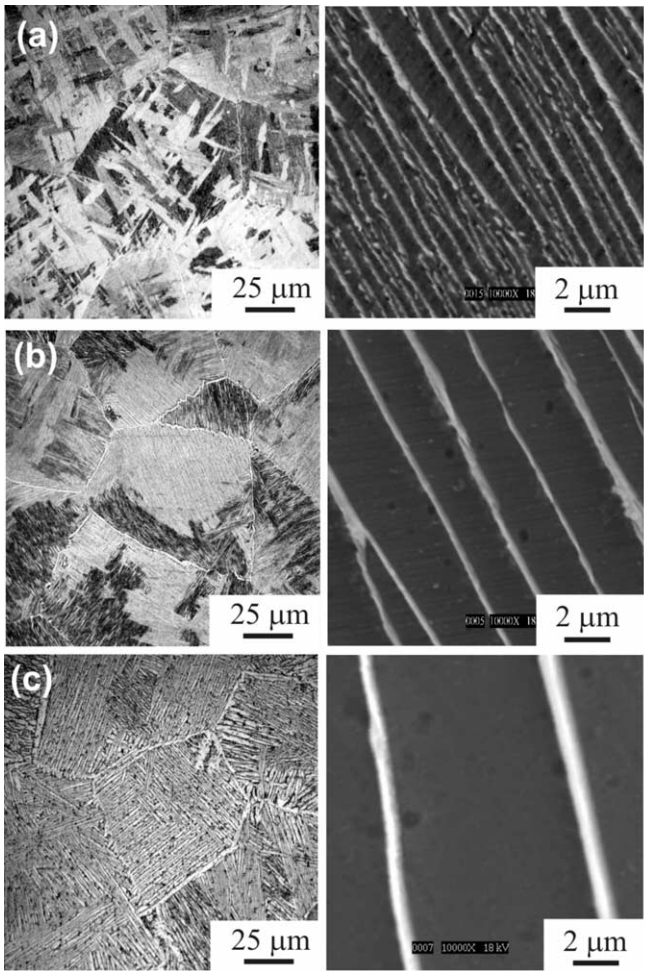

Fig. 2. Microstructure variations as a result of different cooling rates after quenching from β solutioning in Ti6242 alloy. (a) 134 °C min^{-1}. (b) 10 °C min^{-1}. (c) 1 °C min^{-1}.

structures mentioned above. Prior to testing, the specimens were mechanically polished up to 1 μm grad and etched by immersion in Kroll's reagent for 10 s in order to reveal the microstructure details on the flanks of the specimen. Room-temperature precracking was performed at a loading frequency of 20 Hz to obtain a crack length of 0.3 W with a final ΔK value of 14 $MPa\sqrt{m}$. Crack growth was monitored using optical measurements made on both sides of the test specimen. The crack growth was, additionally, monitored using the Potential Drop method, as described in the ASTM Standard [33]. The potential drop curve used in these experiments was calibrated on the basis of optical measurements. All FCG tests were performed on a fully automated servo-hydraulic material testing systems. Heating of the specimens was achieved using a clamshell furnace in which the specimen temperature is controlled by two spot-welded thermocouples. Temperature variations in all tests were maintained less than 5 °C along the specimen height. The crack mouth opening displacement (CMOD) was collected continuously during the

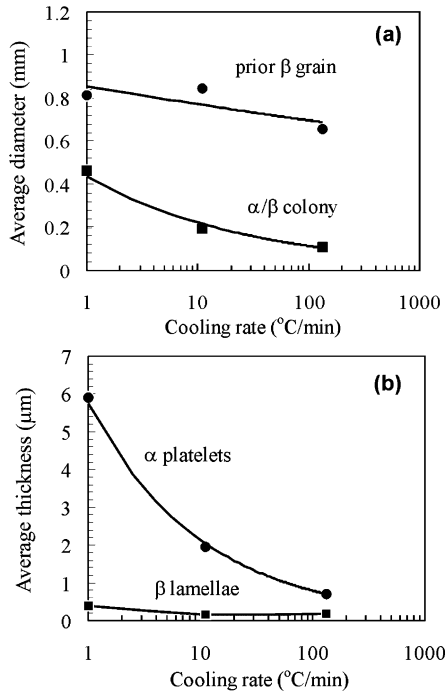

Fig. 3. Effects of cooling rate on the feature dimensions in the three microstructures as presented in Fig. 2.

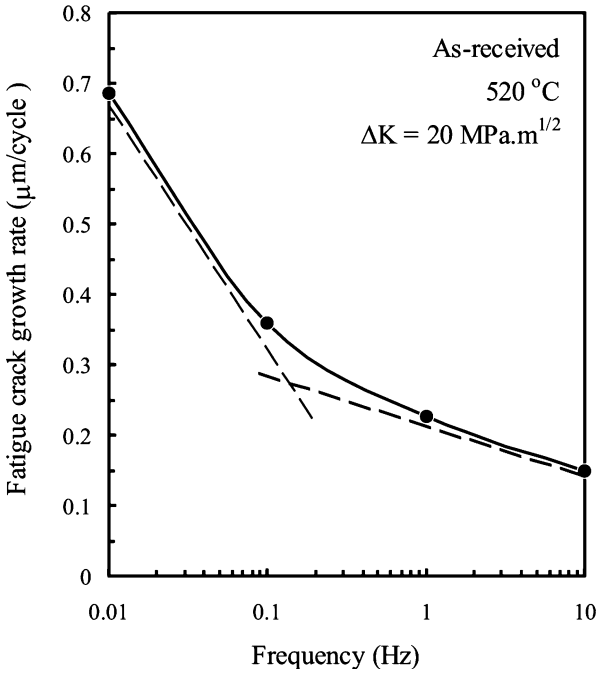

Fig. 4. Effect of loading frequency on the crack growth rate in as-received Ti6242 alloy at 520 °C (constant ΔK test).

test using a high temperature clip gauge. The CMOD measurements were used to determine the effective stress intensity ranges, $\Delta K_{\text{eff}} = K_{\max} - K_{\text{op}}$, where K_{op} corresponds to the stress intensity factor once the crack is fully opened. Crack opening loads were obtained from the plots of the applied load versus the offset-displacements, which are calculated from subtracting the CMOD by the displacements obtained from the slope of the linear portion of the curve. All tests were performed with a constant load ratio, $R = 0.1$. Post-test examinations were conducted by SEM on the fracture surface as well as on the material surrounding the crack path along the two sides of each test specimen.

The effect of loading frequency on the FCG rates was investigated, first, on the as-received microstructure. A test was performed on this microstructure at a constant ΔK value of 20 MPa$\sqrt{\text{m}}$ with a loading frequency varying from 0.01 to 10 Hz. Results of this test are given in Fig. 4. This figure indicates that FCG rate increases as the loading frequency decreases and a significant crack growth rate occurs at frequencies lower than 0.1 Hz. A selection was then made to examine the three microstructures mentioned above using two different frequencies, higher and lower than the 0.1 Hz. These frequencies are 10 and 0.05 Hz. The latter frequency was applied with and without 5 min hold-time being imposed at the maximum load level of each cycle to explore the effects of creep/fatigue interactions. Results of the FCG rates versus applied ΔK for the three microstructures are examined hereafter.

Fig. 5(a) and (b) show the FCG rates versus the applied ΔK for the three microstructures at the loading frequencies of 10 and 0.05 Hz. The addition of a 5 min hold-time seems not to alter the crack growth rate at 0.05 Hz, as shown in Fig. 5(b). This result is similar to data reported in studies investigating creep behavior of titanium alloys. Vesier and Antholovich [34] observed no effects of 30 s hold-time in Ti6242 alloy at 538 °C. Also, Evans and Gostelow [35] found no effects of 5 min hold-time in aligned α microstructure of IMI 685 at 124 °C. Similarly, the work of Sommer and Eylon [36] did not detect any FCG rate acceleration in Ti–6Al–4V tested at room temperature with 5 min hold-time. These results, coupled with the above observation, suggest that creep strain corresponding to 5 min hold time is not sufficient to produce a measurable crack tip fatigue/creep interactions in the lamellar Ti6242. This is also supported by the results of Es-Souni [37] who showed that the total primary creep strain at 500 °C in β-processed Ti6242 alloy is typically less than 0.25 times the elastic strain at a stress of 350 MPa in that material.

Furthermore, Fig. 5(a) shows that the FGC rate at 10 Hz is not significantly influenced by changes in the microstructure. The absence of FCG dependency on microstructure also exists for the 0.05 Hz at ΔK values higher than 30 MPa$\sqrt{\text{m}}$. Below this level, the FCG rate of the fine lamellar microstructure is relatively ΔK independent. This 'plateau' effect, which is less pronounced in the coarse microstructure and almost absent in the extra-coarse microstructure, could be interpreted solely in terms of microstructure variations or, as

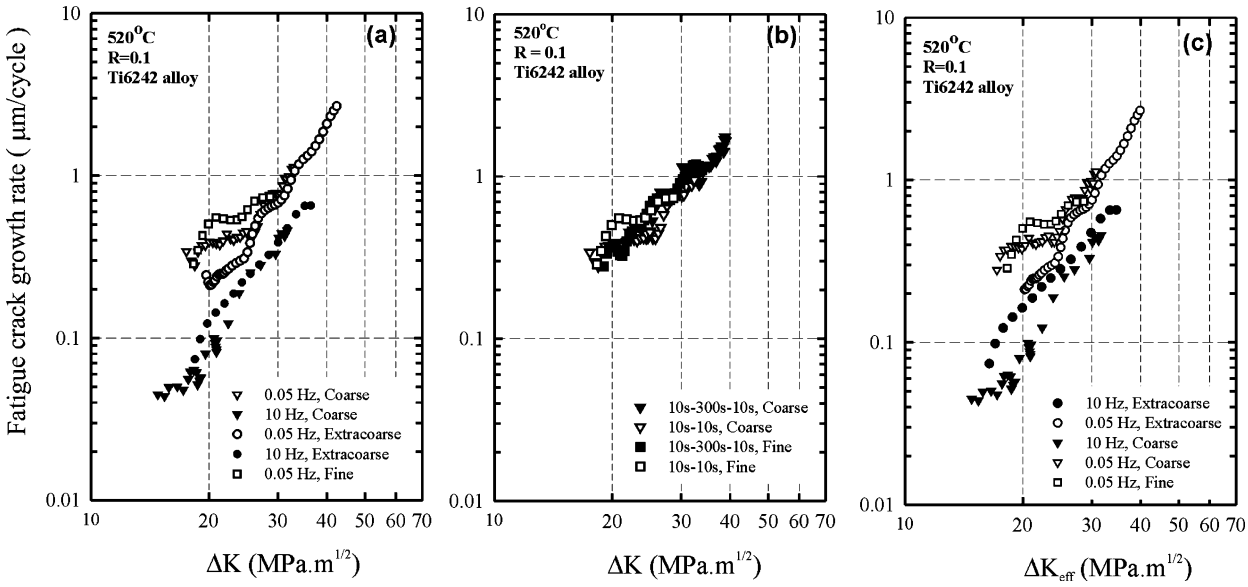

Fig. 5. Fatigue crack growth rate at 520 °C in Ti6242 alloy with colony microstructures as presented in Fig. 2; (a) effects of loading frequency; (b) effects of a 5 min hold-time at peak stress during each loading cycle (0.05 Hz frequency); (c) influence of crack closure effects.

suggested by other authors, could be related to combined microstructure/environment effects. This will be discussed in more details in Section 3.2. The effects of the loading frequency on the cracking process are also represented in Fig. 5(a), where the FCG rate corresponding to 10 Hz loading is lower than that obtained at 0.05 Hz. Several authors have reconciled this type of differences in different titanium alloys by accounting for the crack tip closure effects; see, for example, the work of Ghonem and Foerch [38] on Ti-1100. Fig. 5(c) represents the FCG rate in terms of the effective stress intensity factor ΔK_{eff} determined during the tests. It is observed that taking crack closure effects into account cannot rationalize the differences in crack growth rates observed within the range of explored ΔK value, 17–42 $\text{MPa}\sqrt{\text{m}}$. This is similar to observations made by Sinha and Soboyejo [39] who reported that differences in FCG rate between different colony microstructures in Ti–6Al–4V could not be explained solely by crack closure arguments. Therefore, the FCG differences as observed above, were further investigated by examining the fracture mechanisms associated with the different test conditions. Results of this analysis are discussed in the next section.

3. Analysis and discussion

3.1. Fracture mechanism

The fracture mechanisms associated with the cracking process described above are examined on the basis of SEM observations. The fracture surface was found to promote, in all test conditions, large planar facets presenting a smooth surface character coupled with river lines or, in some cases, striations marks, as shown in Fig. 6(a) and (b), respectively. It is important to note, however, that striations marks were apparent at high ΔK value only (>40 $\text{MPa}\sqrt{\text{m}}$), which is consistent with previous results in large colony microstructures [12,40], and that the crack growth proceeds, to a large extent, by formation of striation-free facets. The orientation of these facets with respect to the microstructure was determined by examining the crack path viewed on both sides of unbroken test specimens. A total of 492 fractured colonies have been explored. Examinations of these colonies revealed two typical fracture modes, transcolony and interboundary. The transcolony fracture corresponds to crack propagation through the entire α/β colony along a path either traversing the lamella or parallel to the lamellae direction as shown in Fig. 7(a) at 10 Hz and Fig. 7(b) at 0.05 Hz, respectively. The parallel-to-lamellae fracture occurs, with no exception, within the α phase with no apparent α/β interface sliding. The second pattern, interboundary fracture, is related to decohesion of intercolony boundaries or prior β grain boundaries; Fig. 8(a) and (b), respectively. The relative occurrence of transcolony and interboundary fractures, obtained from examination of the fractured colony and given in Fig. 9, shows that, under all test conditions performed in this study, the transcolony fracture is a dominant mode of failure. In focusing on this mechanism, one observes that the vicinity of transcolony crack paths displays heavily sheared regions, which were assimilated into intense planar slip bands. Arrows in Fig. 7 show the traces of these slip bands which are parallel to the main crack. The accumulation of planar bands that are generated as a

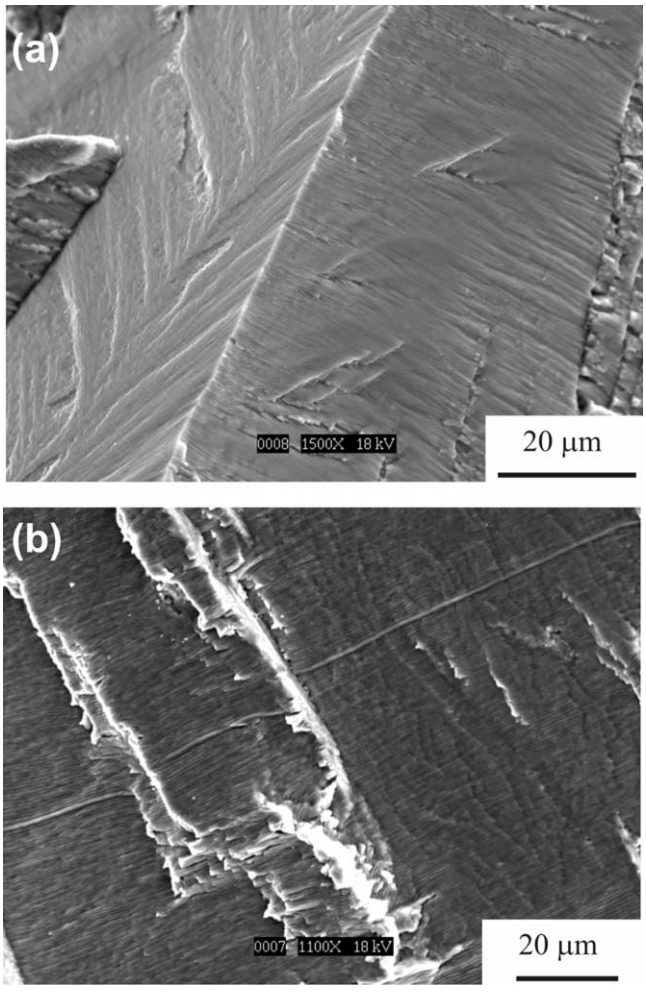

Fig. 6. (a) Typical cleavage-like facets observed at low ΔK. (b) Striations marks at high ΔK value. Note that striations disappear rapidly as the ΔK value is lower than 40 MPa$\sqrt{}$m.

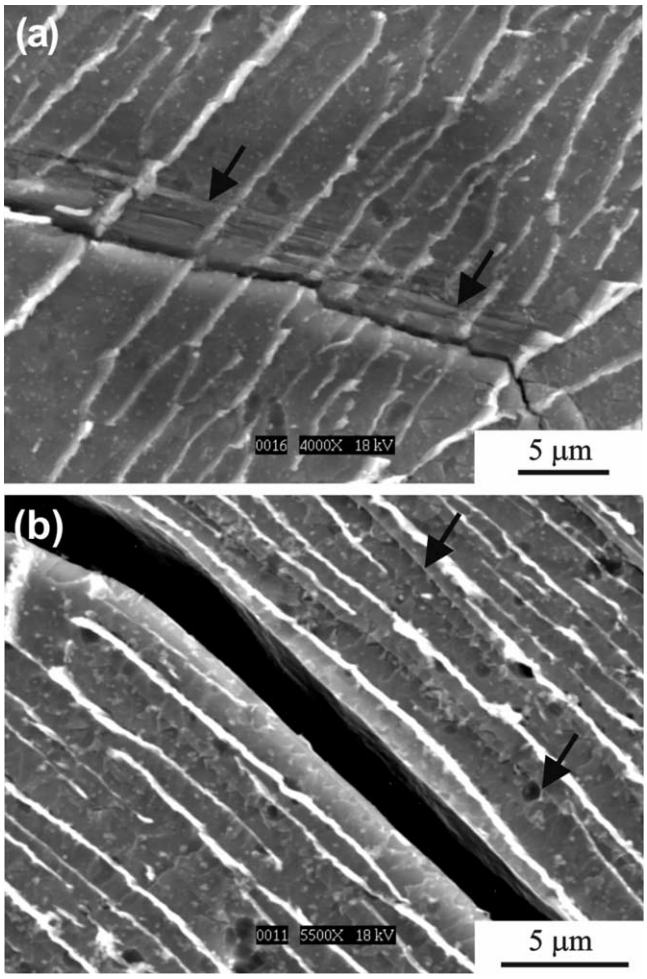

Fig. 7. Transcolony fracture mode in fully lamellar Ti6242 alloy; (a) across α/β lamellae, or (b) parallel to the α/β interfaces. Arrows indicate presence of planar slip traces parallel to the main crack.

result of dislocations emission at the crack tip tends to reduce the transverse strength of the materials within each band [41] and thus allowing the crack to propagate parallel to the band by quasi-cleavage type of fracture. In general, it was observed that the large number of planar slip traces are accompanied with shear offsets at the α/β interfaces, as illustrated by the arrows in Fig. 10. Transverse cracking, particularly at high loading frequency, was also observed along the slip bands, which indicates the possibility of cross-slip within the colony and giving rise to the step-wise planar fracture pattern shown in Fig. 11(a) as well as to crack path bifurcation; see Fig. 11(b). The nature of the planar fracture process and its correlation with the loading frequency is presented below.

Full examination of the planar crack paths has been carried out in the three different microstructures and for the two loading frequencies, 10 and 0.05 Hz. In order to detect a preferential orientation for quasi-cleavage, the angle between the planar crack path and the long axis direction of fractured colonies has been measured. Fig. 12 reports the results of these observations as a function of loading frequency. It shows that the crack path proceeds along two preferential angles formed in relation to the colony long axis. Those angles are near-0° and near-90°, which corresponds to cracking either parallel or perpendicular to the colony geometrical direction. In the following, these will be referred to as parallel crack path and transverse crack path, respectively. Fig. 12 shows, additionally, that reducing the loading frequency leads to a decrease in the tendency in generating transverse crack path and, subsequently, places emphasis on the second mode of failure, i.e. the parallel crack path. It is important to note that the above mentioned tendency was observed independent of the size of the microstructure features within the colony. These results will be interpreted here by considering a qualitative assessment of the interactions between microstructure and crack tip slip behavior as deducted from slip traces observed along the crack path characteristics.

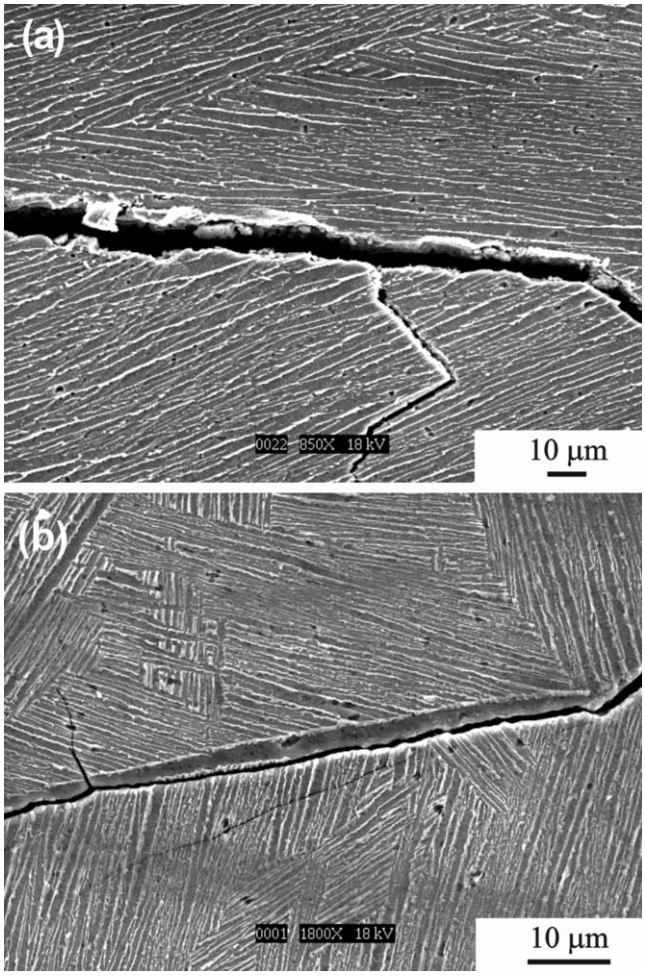

Fig. 8. Interboundary fracture mode observed in fully lamellar Ti6242 alloy; (a) Inter-colony decohesion. (b) Decohesion at prior β grain.

3.2. Results interpretation

The general trend of the slip process as a result of a particular loading condition, particularly, the planar slip, while it is important to observe their corresponding dislocation arrangements via a TEM study, can be identified through the slip traces left on the specimen surface after the fracture events took place. These traces are very well determined using SEM. The planar nature of fracture in our study is also evident by the morphology of the crack path and the cleavage features of the corresponding fracture surface. The relationships between slip character and loading frequency have been studied in details in different high temperature alloys. Cleveringa et al. [42] using discrete dislocation analysis showed that the increase of loading frequency decreases the length of the dislocation motion ahead of the crack tip. Ghonem and Zheng [10] have concluded that the degree of deformation homogeneity becomes more evident at high loading frequency, through the observed low slip line spacing and the confinement of the reversed plastic zone to a narrow band near the crack tip.

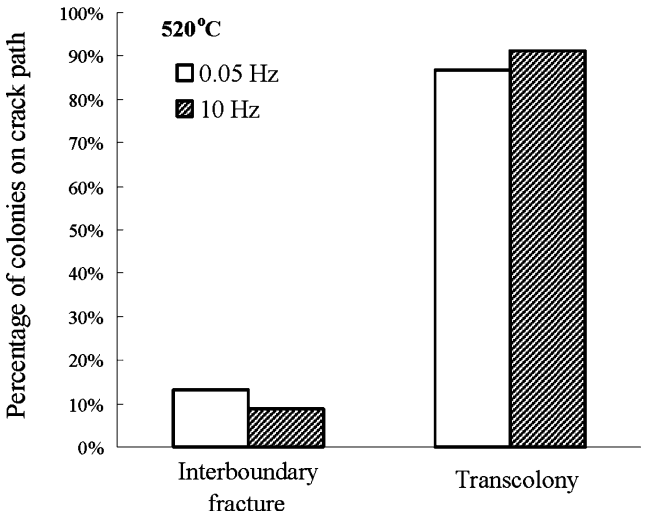

Fig. 9. Probability of cracking at 520 °C in transcolony and interboundary fracture modes as a function of loading frequency.

Increased slip density is known to produce frequent slip interactions between adjacent slip planes [43], resulting in increased cross-slip events which is likely to result in an increased critical resolved shear stress (CRSS) for macroscopic plastic flow and increased hardening in the activated systems. These effects would lead to a lower crack growth rate. It is then suggested that as the CRSS is raised, the degree of deformation anisotropy created at α/β interfaces between different slip systems is homogenized. As the crack growth process in the α/β microstructure is determined mainly by damage events initiating in the α phase, the increased homogenization along the principal slip systems, in the hcp microstructure, could be suggested as basis for the arbitrary crack path illustrated in Fig. 11(a) for 10 Hz. This fracture process contrasts with that associated with low frequencies, which display larger slip line spacing

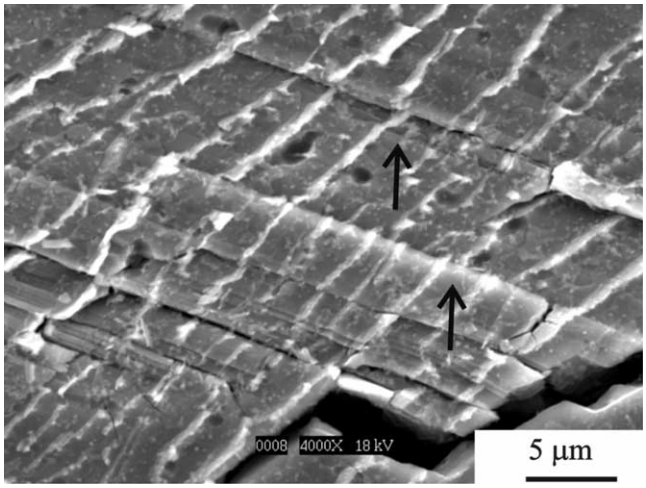

Fig. 10. Typical planar shear bands in the vicinity of a quasi-cleavage crack path. Note the shear offsets at α/β interface indicating the possible existence of prism planar slip.

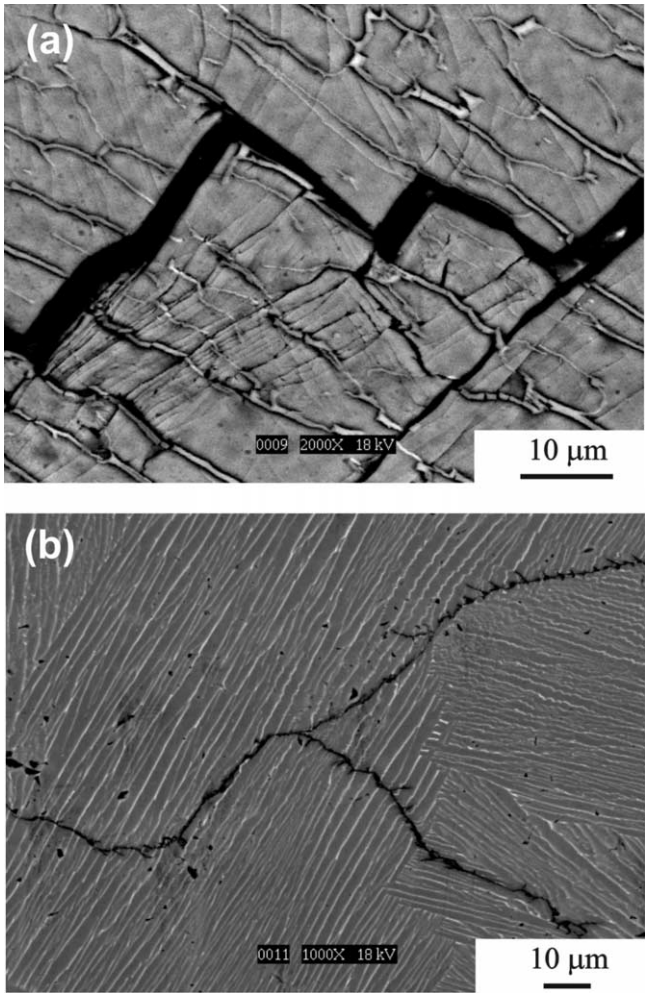

Fig. 11. (a) Step-wise crack propagation along two perpendicular slip systems with a loading frequency of 10 Hz. (b) Crack path bifurcation within an individual α/β colony at 10 Hz. (both micrographs taken using backscattered electron emission).

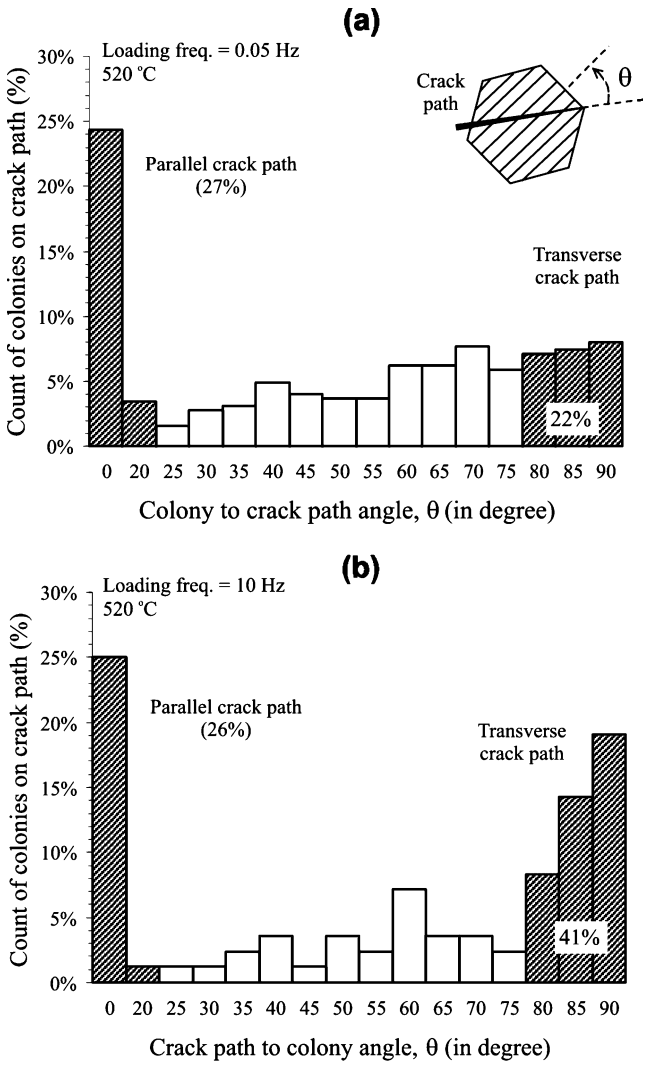

Fig. 12. Orientation of cracking with respect to the colony long axis direction at two different loading frequencies: (a) 0.05 Hz. (b) 10 Hz.

evident by the surface traces shown in Fig. 7(b), when compared with that associated with high frequency loading, see Fig. 7(a). The larger the slip line spacing, the lower the possibilities of cross-slip events, and the lower the CRSS, which would then promote fracture along a preferential slip system.

The ground for interpreting the selection in crack path orientation with respect to the loading frequency is based on results of earlier TEM investigations in conjunction with the fatigue crack tip slip emission in large colony Ti microstructures [11]. It was found in this class of microstructure that the crack tip was subjected to two shear modes on the α basal (0001) plane and the α prismatic $\{10\bar{1}0\}$ plane, with all dislocations on both planes to be of the $\langle a\rangle$-type ($\langle 11\bar{2}0\rangle$). The typical configuration of these dislocations was found to be a pile-up at the α/β interfaces, thus applying a substantial stress on the interface. The breakdown of the very first barrier enables doubling the pile-up length and the shear band propagates to the end of the colony. In the work of these authors, the crack initiation, the crack propagation and the last stage of propagation appeared to be dominated by the same shear activity. One may consider the possible shear activity associated to transverse and parallel crack path configurations, as illustrated in Fig. 7(a) and (b), respectively, by assuming perfect Burgers' relationships between α-Ti and β-Ti platelets [6,44]; $(101)_\beta \| (0001)_\alpha$ and $[1\bar{1}\bar{1}]_\beta \| [2\bar{1}\bar{1}0]_\alpha$ and, particularly by keeping in mind that the α phase [0001] c-axis is quasi-parallel to the β platelets long axis direction [44], as illustrated schematically in Fig. 13. Consequently, there is a possibility that shear activity in the parallel crack path configuration may be attributed to $\langle a\rangle$-slip in $(01\bar{1}0)$ prism plane or, eventually, to $\langle c+a\rangle$-slip in various pyramidial planes of the α phase; see Fig. 13(a). On the other hand, shear in transverse crack path configurations, which could not coincide with $(01\bar{1}0)$ prism slip, may be relevant to shear activity along (0001)

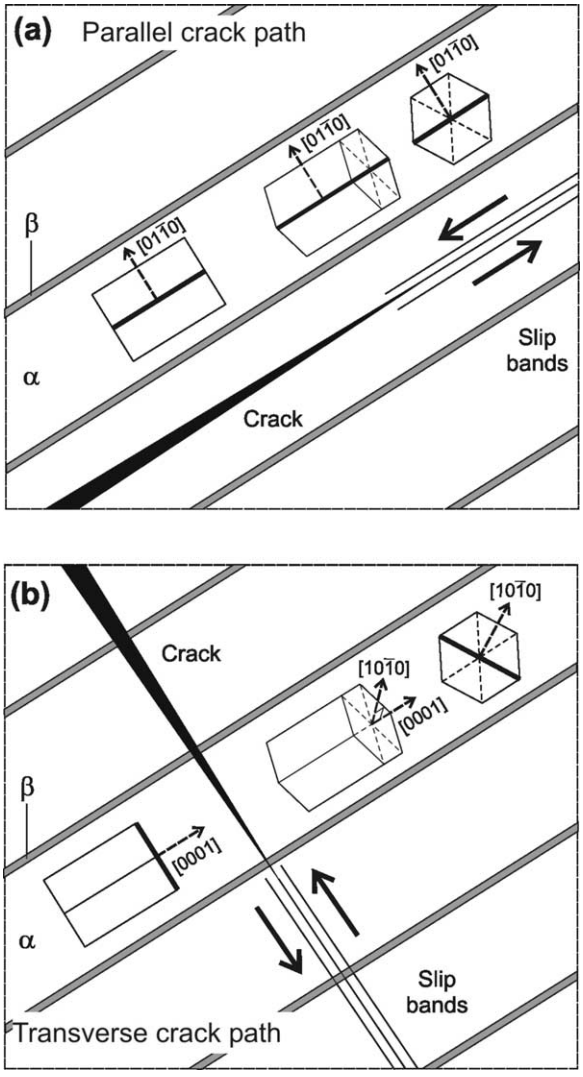

Fig. 13. Schematic showing (a) parallel crack path and (b) transverse crack path with respect to the orientation of the hcp α-Ti unit cell, in colonies promoting perfect Burgers' relationship between α and β platelets. Note that the (0001) c-axis of the α unit cell is always parallel to the β platelets.

basal slip, $(10\bar{1}0)$ prism slip or, eventually, pyramidial slip; see Fig. 13(b). Different investigations [45,46] have demonstrated on monotonic testing of Ti alloys with an aluminum concentration $\geq 6\%$, that pyramidial slip is limited as a deformation mode above 500 °C as compared to basal and prism slips. Moreover, the possibility of slip occurring along any of these prism or basal directions is generally determined by the corresponding CRSS. Williams et al. [46] have shown that the CRSS of prism planes are generally lower than that of the basal plane. The differences in the CRSS values between these two slip systems, however, decrease as the temperature increases. Mills and co-workers [44,47,48] have examined the CRSS values of the basal and prism slips in the three $\langle 11\bar{2}0\rangle$ directions by micro-tensile testing in individual α/β colonies of Ti6242 and different α/β Ti alloys at room temperature, and have shown that, in contrast to the $(10\bar{1}0)$ prism slip, the residual dislocations in the $(01\bar{1}0)$ prism plane were small, thus leading to a low CRSS and low work hardening rate in that direction. It is worth noting here that $(01\bar{1}0)$ prism slip always impinges the α/β interface with a shallow angle, while both (0001) basal slip and $(10\bar{1}0)$ prism slips form a very large angle to this interface.

Based on the previous observations and considering that low frequency conditions promote little cross-slip interactions as found at 0.05 Hz, it could be argued that, due to the anisotropy in slip transmission created at the α/β interfaces, the slip length is likely more limited in transverse direction; i.e. in shear activity along (0001) basal or $(10\bar{1}0)$ prism slips, than in the parallel direction; i.e. in shear activity along $(01\bar{1}0)$ prism slip; see Fig. 13. It is therefore proposed that the lower the loading frequency, the more extended the reversed plastic zone and the more representative of the length and the flow rate of parallel-to-lamella shear band the FCG rate. The suggested correlation between slip density and fracture mechanisms in both high and low frequency loading is schematically illustrated in Fig. 14. It should be mentioned here that in the cracking modes associated with the two loading frequencies, the slip is considered limited to the crack tip plastic zone, which even at high value of ΔK and low loading frequency, is bounded by the colony boundary, see Fig. 15.

In order to confirm the significance of the slip homogeneity on the FCG rates, an attempt was made to create obstructions along one of the preferential slip directions and examine the resulting crack growth rate corresponding to high and low frequency loading. This is achieved by precipitating small α needles within the β lamellae to make the slip transmission in the transverse direction more difficult. The heat treatment proposed by Wegmann et al. [49] in Ti6242 alloy was used in this work. This treatment consists in the addition of an annealing treatment at 970 °C for 1 h just after the solutioning treatment followed by a 300 °C min^{-1} cooling. This technique was performed on a coarse lamellar microstructure resulting in a bilamellar microstructure that is shown in Fig. 16(a). The resulting β lamellae size is equal to 0.6 μm and precipitation of small-unaligned α needles are observed within the β lamellae, as shown in this figure. Crack growth test were carried out on this bilamellar microstructure at 10 and 0.05 Hz following the same test procedure previously described. Results are presented in Fig. 16(b). In this figure, the FCG rates obtained at low frequency are identical in coarse and bilamellar microstructures as expected since predominantly parallel crack path is followed at this loading frequency. On the other hand, at high frequency where both slip directions are active cracking path, the FCG rate is higher in bilamellar than

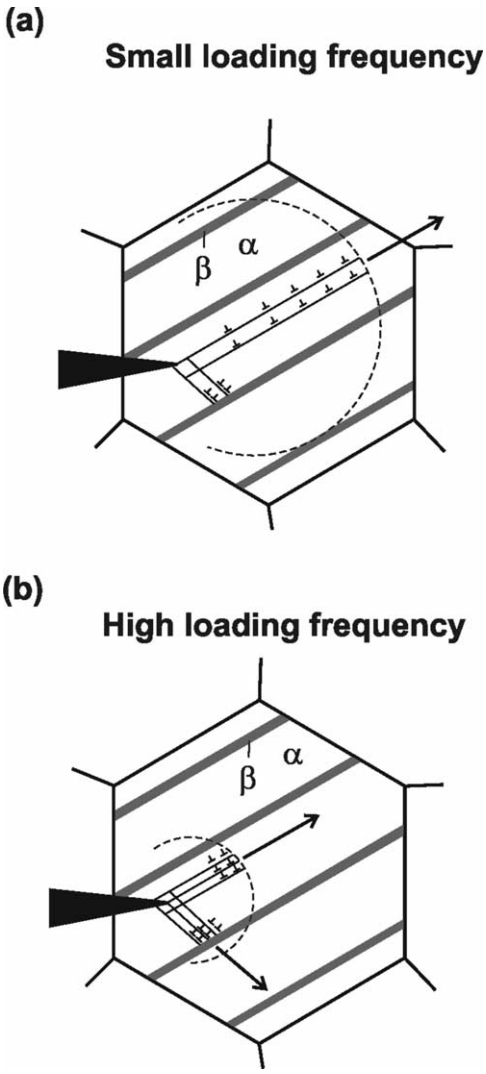

Fig. 14. Schematic illustrating the influence of loading frequency based on possible crack tip slip emission. Note that at low loading frequency, it is believed that the α/β interface restricts the shear activity in the direction transverse to this interface. The dotted circle represents the extent of crack tip cyclic plasticity within one colony, and the arrows indicates preferential crack path direction.

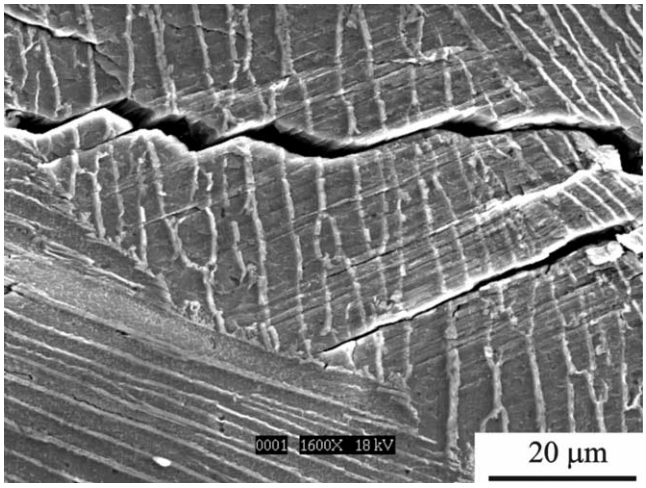

Fig. 15. The crack tip region at $\Delta K = 30$ MPa$\sqrt{}$m and low loading frequency showing the flow of slip band traces being restricted by an α/β colony boundary.

in coarse microstructure. This result indicates that the α precipitates within the β phase obstructed the transverse slip, forcing parallel crack path to become the dominant fracture mode as shown in Fig. 16(c). At high ΔK values, however, the difference in the FCG rates is less significant as the fracture process will be more dependent on the ΔK and less sensitive to the slip behavior at the crack tip.

The mechanism of crack tip slip emission proposed above, however, cannot be used to explain the presence of 'plateau' and the differences in the FCG rates between the three microstructures at low ΔK levels and low loading frequency, since parallel crack path, as observed with this regime, does not intersect the lamellae. Ruppen et al. [40] in their work on Ti6242 alloy at 540 °C, have observed that 'plateau' effects at low ΔK level are eliminated under high vacuum conditions, which suggests that combined effects between microstructure and environment may operate in the present study. Similar results have been reported in lamellar microstructures of Ti–6Al–4V alloy at 350 °C by Schroeder et al. [50] and up to 300 °C by Sarrazin-Baudoux et al. [51]. Ruppen and McEvily [52], however, did not detect notable effect of microstructure in Ti6242 alloy at 540 °C with high fatigue loading frequency. The onset of localized plasticity is often related to the presence of hydrogen in inhibiting the dislocation pile-up relaxation and increasing the mobility of dislocations in Ti alloys [53,54]. There is, however, very little support to this hypothesis in the present work due to the fact that no significant hydrogen embrittlement has been detected at temperatures higher than 350 °C in titanium alloys [8,38]. Further, quasi-cleavage facets dominate the fracture surface in all testing conditions. This strongly suggests that the accelerated formation of the facets, which is often related with the increase in Ti_3Al particles volume fraction with increasing oxygen content or aging duration [46,55–57], may be due to oxygen diffusion at the crack tip [56]. In this condition, a complex interaction would exist between the depth of oxygen diffusion and the crack tip cyclic zone size. Microstructure geometries, particularly the lamella size, as well as the loading frequency and test temperature directly affect these two damage effects. The full understanding of the role of each of these parameters on the enhancement of the diffusion assisted crack growth process could be achieved through the numerical simulation of the cracking mechanisms in the α/β colony. The authors are currently carrying out a

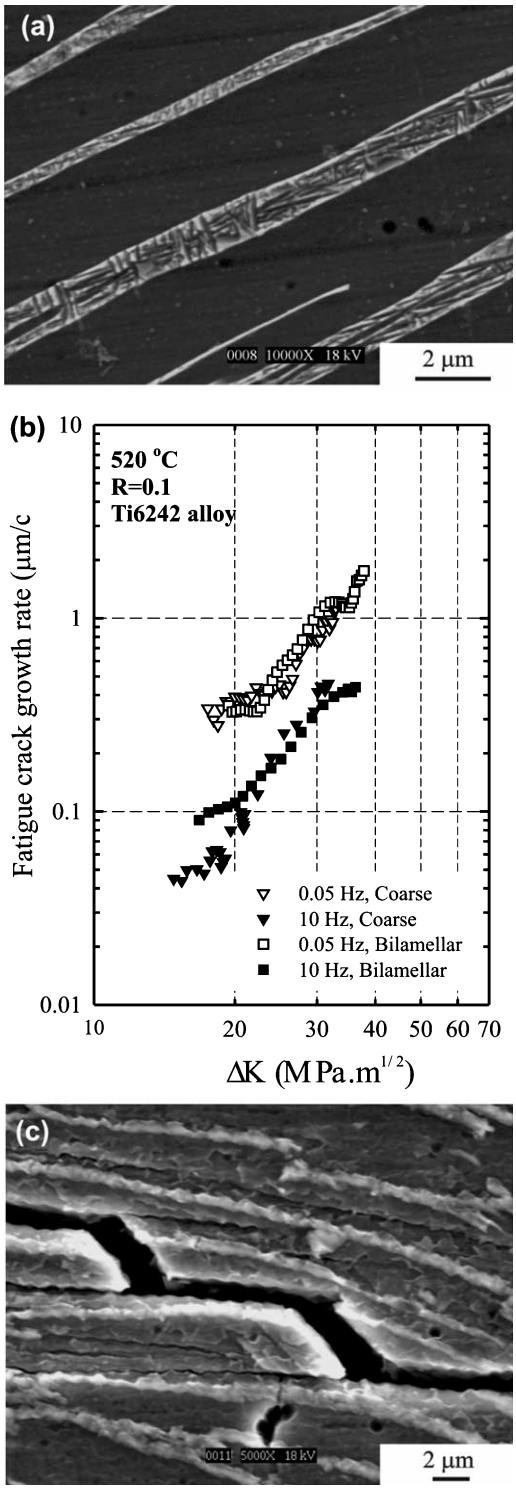

Fig. 16. (a) Bilamellar microstructures with identical colony size and α platelets size than coarse microstructures. Note that the size of β lamellae is significantly increased to impede the slip emission in the transverse direction. (b) Influence of loading frequency on FCG rate. (c) Typical parallel-to-lamella crack path observed at 10 Hz in bilamellar microstructure.

numerical study aiming at examining the microstructure/oxygen diffusion interactions in α/β lamellar titanium alloys.

4. Summary and conclusions

Three fully lamellar microstructures of Ti6242 alloy with large colony size (>0.1 mm) were examined in this study. FCG experiments were conducted on these microstructures to determine the influence of small loading frequency (0.01–10 Hz) on the associated FCG mode of failure. All tests were performed at 520 °C with a stress ratio of 0.1 in air environment. Results of this investigation lead to the following conclusions:

- The FCG rate at 10 Hz is not significantly influenced by changes in the microstructure. This behavior of microstructure independency also exists for the 0.05 Hz at high values of ΔK. At low ΔK the crack growth rate of the fine lamellar microstructure at 0.05 Hz, shows a plateau effect. It is suggested that microstructure/environment interactions may have resulted in this effect. Moreover, the addition of a 5 min hold-time at the maximum load level does not alter the crack growth rate. It is assumed that the creep strain corresponding to 5 min is not sufficient to produce crack tip fatigue/creep interaction effects in the lamellar Ti6242 at 520 °C. Further experiments at higher temperature are currently underway by the authors in order to explore effects of higher levels of creep strain on the crack growth process.
- Under all test conditions performed in this study, the quasi-cleavage of α/β colony along intense planar shear bands is the predominant mode of failure. The orientation of the shear band activity is seen influenced by the loading frequency. At 10 Hz, shear activity is observed either parallel or quasi-perpendicular to the lamella long axis direction. In contrast, while decreasing the loading frequency to 0.05 Hz, shear activity in a perpendicular-to-lamella mode is diminished. It is argued based on existing observations of the slip emission at crack tip that α/β interface may hinder the shear activity in transverse configuration aided by the reduced plastic flow rate in the associated direction at small loading frequency. When the frequency increases, the slip line density increases and the size of the reversed plastic zone at the crack tip decreases, resulting in increased cross-slip interactions, thus leading to lower crack growth rates.
- The significance of the shear activity on the FCG rate is pointed out by performing high and low frequency crack tests on bilamellar microstructure in which small-unaligned α needles are precipitated within the β lamellae. The FCG rates obtained at low frequency is identical in coarse and bilamellar microstructures since predominantly parallel crack paths are followed at this loading frequency. At high loading frequency where both parallel and transverse shear directions

are considered active cracking paths, the α precipitates within the β phase obstructed the transverse slip, forcing parallel crack path to become the dominant fracture mode. As a result, the FCG rate is higher in bilamellar than in coarse microstructure.

Acknowledgements

The authors would like to acknowledge SNECMA, Etablissement de Villaroche, France for the financial and material support of this study. Dr Jean-Yves Guedou of SNECMA is the program manager.

References

[1] R.R. Boyer, Mater. Sci. Eng. A213 (1996) 103–114.
[2] S.L. Semiatin, J.F. Thomas, Jr, P. Dadras, Metall. Trans. A 14A (1983) 2363–2374.
[3] C.C. Chen, J.E. Coyne, In: H. Kimura and O. Izumi (Eds.), Titanium 80 Science and Technology, Proceedings of the 4th International Conference on Titanium, vol. 2, Kyoto, Japan, The Metallurgical Society of AIME, Warrendale, PA, USA, 1980, pp. 1197–1207.
[4] D. Eylon, J.A. Hall, C.M. Pierce, D.L. Ruckle, Metall. Trans. A 7A (1976) 1817–1976.
[5] W.J. Evans, Mater. Sci. Eng. A243 (1998) 89–96.
[6] J.A. Ruppen, C.L. Hoffmann, V.M. Radhakrishnan, A.J. McEvily, in: J.J. Burke, V. Weiss (Eds.), Fatigue, Environment and Temperature Effects, Plenum Press, New York, 1980, pp. 265–299.
[7] H.J. Maier, Mater. High Temp. 15 (1) (1998) 3–14.
[8] J.K. Gregory, in: A. Carpinteri (Ed.), Handbook of Fatigue Crack Propagation in Metallic Structures, Elsevier Science, New York, 1994, pp. 281–322.
[9] G. Lütjering, Mater. Sci. Eng. A243 (1998) 32–45.
[10] G.R. Yoder, L.A. Cooley, T.W. Crooker, J. of Eng. Mater. Tech. (October 1977) 313–318.
[11] D. Shechtman, D. Eylon, Metall. Trans. A 9A (1978) 1018–1020.
[12] G.R. Yoder, L.A. Cooley, T.W. Crooker, Metall. Trans. A 8A (1977) 1737–1743.
[13] G.R. Yoder, L.A. Cooley, T.W. Crooker, Metall. Trans. A 9A (1978) 1413–1420.
[14] D. Eylon, J.A. Hall, Metall. Trans. A 8A (1977) 981–990.
[15] P.J. Bania, D. Eylon, Metall. Trans. A 9A (1978) 847–855.
[16] D. Eylon, P.J. Bania, Metall. Trans. A 9A (1978) 1273–1279.
[17] D.L. Davidson, D. Eylon, Metall. Trans. A 11A (1980) 837–843.
[18] A. Yuen, S.W. Hopkins, G.R. Leverant, C.A. Rau, Metall. Trans. 5 (1974) 1833–1842.
[19] K.S. Ravichandran, Acta Metall. Mater. 39 (3) (1991) 401–410.
[20] C. Choi, Y.T. Lee, C.S. Lee, Scripta Mater. 36 (7) (1997) 821–827.
[21] D. Eylon, T.L. Bartel, M.E. Rosenblum, Metall. Trans. A 11A (1980) 1361–1367.
[22] H. Ghonem, D. Zheng, Metall. Trans. A 23A (1992) 3067–3072.
[23] R. Foerch, A. Madsen, H. Ghonem, Metall. Trans. A 24A (1993) 1321–1332.
[24] A.H. Rosenberger, H. Ghonem, Fatigue Fract. Eng. Mater. Struct. 17 (4) (1994) 397–410.
[25] B. Odegard, A.W. Thomson, Metall. Trans. 5 (1974) 1207–11213.
[26] S. Lesterlin, C. Sarrazin-Baudoux, J. Petit, Scripta Mater. 34 (4) (1996) 651–657.
[27] Y.T. Hyun, Y.T. Lee, W.J. Evans, C.G. Lee, High Temp. Mater. Process. 20 (1) (2001) 17–23.
[28] S.J. Gao, G.W. Simmons, R.P. Wei, Mater. Sci. Eng. 62 (1984) 65–78.
[29] N.R. Moody, W.W. Gerberich, Metal Science (March 1980) 95–100.
[30] S.L. Semiatin, V. Seetharaman, I. Weiss, JOM (June 1997) 33–39.
[31] J. Lindeman, L. Wagner, Mater. Sci. Eng. A263 (1999) 137–141.
[32] S.L. Semiatin, J.C. Soper, I.M. Sukonnik, Scripta Metall. Mater. 30 (7) (1994) 951–955.
[33] D. Zheng, Ph.D. thesis, University of Rhode Island, Kingston RI, USA, 1992.
[34] L.S. Vesier, S.D. Antolovich, Eng. Fract. Mech. 37 (4) (1990) 753–775.
[35] W.J. Evans, C. Gostelow, Metall. Trans. A 10A (1979) 1837–1846.
[36] A.W. Sommer, D. Eylon, Metall. Trans. A 14A (1983) 2178–2181.
[37] M. Es-Souni, Mater. Charact. 45 (2000) 153–164.
[38] H. Ghonem, R. Foerch, Mater. Sci. Eng. A318 (1) (1991) 69–81.
[39] V. Sinha, W.O. Soboyejo, Mater. Sci. Eng. A319-321 (2001) 607–612.
[40] J.A. Ruppen, A.J. McEvily, In: L.N. Gilbertson and R.D. Zipp (Eds.), Fractography and Materials Science, ASTM STP 733, American Society for Testing and Materials, 1981, pp. 32–50.
[41] J.A. Hall, Int. J. Fatigue 19 (Suppl. 1) (1997) S23–S37.
[42] H.H.M. Cleveringa, E. Van Der Giessen, A. Needleman, Mater. Sci. Eng. A317 (2001) 37–43.
[43] K.S. Chan, C.C. Wojcik, D.A. Koss, Metall. Trans. A 12A (1981) 1899–1907.
[44] M.F. Savage, J. Tatalovich, M. Zupan, K.J. Hemker, M.J. Mills, Mater. Sci. Eng. A319–321 (2001) 398–403.
[45] G. Welsch, W. Bunk, Metall. Trans. A 13A (1982) 889–899.
[46] J.C. Williams, R.G. Baggerly, N.E. Paton, Metall. Trans. A 33A (2002) 837–850.
[47] S. Suri, T. Neeraj, D.H. Daehn, D.H. Hou, J.M. Scott, R.W. Hayes, M.J. Mills, Mater. Sci. Eng. A234–236 (1997) 996–999.
[48] S. Suri, G.B. Viswanathan, T. Neeraj, D.H. Hou, M.J. Mills, Acta Mater. 47 (3) (1999) 1019–1034.
[49] G. Wegmann, J. Albrecht, G. Lütjering, K.D. Folkers, C. Liesner, Z. Metallkd. 88 (10) (1997) 764–772.
[50] G. Schroeder, J. Albrecht, G. Luetjering, Mater. Sci. Eng. A319–321 (2001) 602–606.
[51] C. Sarrazin-Baudoux, S. Lesterlin, J. Petit, In: R.S. Piascik, R.P. Gangloff, A. Saxena (Eds.), Elevated Temperature Effects on Fatigue and Fracture, ASTM STP 1297, American Society for Testing and Materials, 1997, pp. 117–139.
[52] J.A. Ruppen, A.J. McEvily, Fatigue Fract. Eng. Mater. Struct. 2 (1979) 63–72.
[53] H.K. Birnbaum, P. Sofronis, Mater. Sci. Eng. A176 (1994) 191–202.
[54] J.K. Gregory, H.-G. Brokmeier, Mater. Sci. Eng. A203 (1995) 365–372.
[55] J.Y. Lim, C.J. McMahon, Jr, D.P. Pope, J.C. Williams, Metall. Trans. A 7A (1976) 139–144.
[56] G.T. Gray, G. Luetjering, J.C. Williams, Metall. Trans. A 21A (1990) 95–105.
[57] T. Neeraj, M.J. Mills, Mater. Sci. Eng. A319–321 (2001) 415–419.